CONFORMAL TISSUE SCAFFOLD WITH MULTI-FUNCTIONAL POROSITY FOR WOUND HEALING

AKM Bashirul Khoda[1], Bahattin Koc[2]*

[1] University at Buffalo (SUNY), Buffalo, NY 14260, USA
[2]Sabanci University, FENS G013, Orhanli-Tuzla, Istanbul, 34956, Turkey

ABSTRACT: In tissue engineering and wound healing, porous scaffolds can stimulate the wound healing process by regenerating the damaged or diseased tissue. But when applied in wound area various forces like bandage, contraction and self weight act upon these visco-elastic scaffold/membrane and cause deformation. As a result, the geometry and the designed porosity change which eventually alters the desired choreographed functionality such as material concentration, design parameters, cytokines distribution over the wound device geometry. In this work, a novel scaffold modelling approach has been proposed that will minimize the change in effective porosity with the designed porosity due to its deformation. First the targeted wound surface model has been extracted and sliced along its depth. Then the height based contours are projected and descritized into functional regions Surface profile for each region have been extracted with contour area weight based slope method. Finally, the filament deposition locations have been generated considering the region profile. Thus the proposed method will give a better functionality of tissue membrane providing predictable material concentration along the wound surface and optimum environment under deformed conditions. The methodology has been implemented using a bi-layer porous membrane via computer simulation. A comparison of the results of effective porosity between the proposed design and conventional design has also been provided. The result shows a significant improvement and control over desired porosity with the proposed method.

KEYWORDS: Scaffold design, Porosity, Spatial material concentration.

1 INTRODUCTION

Bi-layer porous membrane such as guided tissue regeneration (GTR) membrane, cell sheet, tissue matrix or polymeric mesh [1] are being widely used in different types of wound (e.g. acute, chronic, exuding and dry wounds, etc.) for the purpose of expediting the wound healing process in the form of wound dressing and/or drug delivery. In many instances, these synthetic matrices/scaffolds/ membranes seeded with or without cell are often equipped with wound healing accelerators called biofactors (e.g., growth factors, cytokines, and DNA fragments) and combined with synthetic and/or natural materials for synergic beneficial aspects [2] which are called composite or hybrid scaffolds [3]. Not only those structures should be biodegradable, biocompatible, non-cytotoxic and non-antigenetic [1], but also they must have physical agility (e.g. pliability, elasticity) [4] for proper adherence, ease of application and removal, avoid wrinkling or fluting [2].

Currently homogeneous membrane/scaffolds are being used by practitioner to expediting the wound care in the form of dermal wound dressing, bi-laminate facial mask, burn wound covering membranes [5]. The filaments are assumed to be solid and filaments. But when applied in wound area, various forces caused by bandage or occlusive dressing [6], contraction due to vacuum assisted (wound) closure (VAC) [7], curvature of the skin, and/or self weight act upon the visco-elastic membrane might cause deformation. As a result, the geometry and the intended porosity might change which eventually alter the vital characteristics such as material concentration, design parameters, cytokines distribution over the wound membrane geometry. This could jeopardize the choreographed functionality affecting the wound environment, triggering inflammatory response and reversing the wound healing process.

In this paper, we evaluate the affect of deformation of membrane/dressing discussed earlier on the resultant porosity of the membrane/dressing. The porosity is a critical factor for the device functionality and such deformation alter the designed material concentration/porosity and might have adverse affect on the wound micro environment. To avoid such affect a novel scaffold modelling approach of desired porosity with variational filament distance has been proposed. Thus the proposed method will give a better functionality of such membrane providing predictable material concentration along the wound surface. The methodology has been implemented in this paper and illustrative examples are provided via computer simulation. To measure the effectiveness of the proposed model, the shape conforming deformation has been modeled via finite element analysis (Abaqus 6.9) using the hydrogel material properties. A comparison of resultant porosity between proposed design model and conventional fixed filament distance model has been presented via virtual bi-layer membrane applied on free-form surface mimicking wound.

* Corresponding author: Faculty of Engineering and Natural Sciences, Sabanci University, FENS G013, Orhanli-Tuzla, Istanbul, 34956, Turkey. Tel.: +902164839557; fax: +90 2164839550.E-mail address: bahattinkoc@sabanciuniv.edu (B. Koc).

2 BI-LAYER MEMBRANE WITH CONTROLLABLE POROSITY

In the literature, majority of the synthetic membrane fabricated with 3D printing/layered-based manufacturing techniques are designed with uniform porosity level via a fixed filament distance throughout the structure because of design and manufacturing limitations [8, 9]. For such uniform membrane, the porosity can be calculated from the unit cell assumption and obtained as a function of fibre diameter (D) and spaces between fibres (L) by the following equation [10].

$$P = 1 - \frac{\pi D}{4L} \qquad (1)$$

Now applied forces on such visco-elastic membrane might cause a shape conforming deformation over the wound profile. Moreover because of the strain in the filament, the diameter would change and so as the designed porosity as shown in Figure 1. And thus with the same volume of material and increased in surface area, the resultant spatial material concentration decreases which eventually increases the final effective porosity.

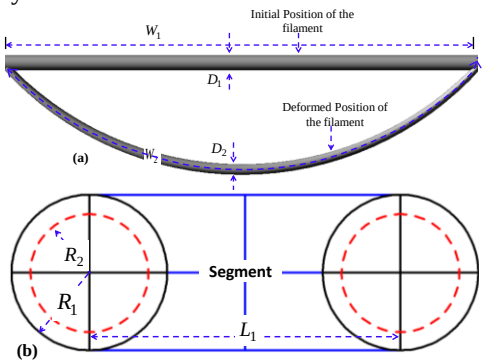

Figure 1: *Change in filament (a) length and (b) corresponding diameter due to the deformation.*

2.1 SLICING THE MODEL AND GENERATING STRIPS

Firstly, medical image obtained from Computed Tomography (CT), Magnetic Resonance Imaging (MRI) or reverse engineering is used to obtain the geometric and topology information of the wound shape. The 3D wound model then sliced by a set of intersection plane perpendicular to the depth of the surface to find the slicing contours $S = \{s_i\}$, where i is the number of contour slice for the wound geometry. Contours were generated by connecting the intersection points between the plane and the surface. Then these height/ depth specified sliced contour are projected as a set of projected contours $P_s = \{P_{s_i}\}$ on the wound top-plane and a set of parallel line $SL = \{SL_j\}$ have been drawn along the lay-down direction to discretize those projected contours. The distance between such intersecting lines can be uniform $d\_SL_i = d\_SL_j \quad \forall i, j$ or variational $d\_SL_i \neq d\_SL_j \quad \forall i, j$ and must be greater than the width of a single segment, $d\_SL_i > \text{Segment\_width} \quad \forall i$ shown in Figure 2. Area generated between two adjacent parallel lines has been noted as strips $ST = \{ST_{j+1}\}$ and the effective area for k^{th} strip can be defined as the area generated by the outer most projected contour in that strip i.e. $ST_k^{eff} = \{ST_k \cap P_{S_{i=S}}\}$ as shown in Figure 2.

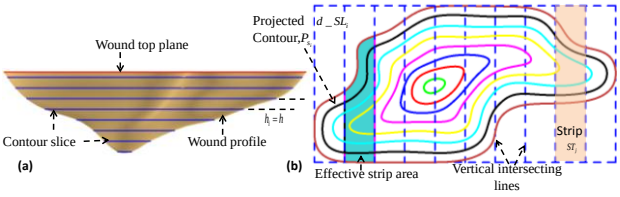

Figure 2: *(a) Generating height base contour (b) strips.*

Both the number of height/ depth specified sliced contour and number of strips can be considered as controllable design parameters which can be represented as quadratic function for wound surface approximation and can be represented by the following equation.

$$\alpha L \leq (d\_SL + h) \leq \beta L \quad \forall\ 1 < \alpha \leq \beta \qquad (2)$$

Where, the two controllable parameter i.e. strip width, d_SL and slice distance, h have been combined $(d\_SL + h)$ together and the two uncontrollable parameter i.e. porosity and filament radius have been replace by a single parameter L i.e. distance between filament in conventional membrane and can be calculated by using Equation 1. α and β are the constants that determine the upper and lower range of the combined controllable parameters based on the remaining uncontrollable parameters. For a complex wound surface, the value of $(d\_SL + h)$ should lie towards the lower range and vice versa.

2.2 OPTIMUM FILAMENT LOCATION

To approximate the free form wound surface profile with three dimensional point location, a contour area based average surface normal angle determination methodology [1] has been applied where the set of slicing contour S from previous section act as guiding contours.

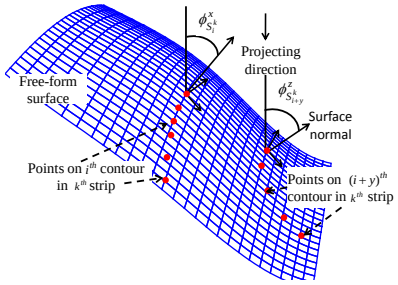

Figure 3: *Measuring the surface normal along the projected contour and wound profile.*

If k^{th} strip has intersection with n_k number of projected contour, then the resultant surface normal for that strip, can be calculated by the following equation,

$$\phi_{avg}^{k} = \left(\sum_{i}^{n_k-1} \left|\phi_{S_i^k}\right|_{eff} \times \frac{P_{S_i}^{k} - P_{S_{i+1}}^{k}}{ST_k^{eff}}\right) + \left(\left|\phi_{S_{n_k}^k}\right|_{eff} \times \frac{P_{S_{n_k}}^{k}}{ST_k^{eff}}\right) \forall\ k \quad (3)$$

$$\left|\phi_{S_i^k}\right|_{eff} = \frac{\sum_{x=1}^{N_i^k} \phi_{S_i^k}^{x}}{N_i^k = \left(\frac{P_{S_i}^{k} - P_{S_{i+1}}^{k}}{ST_k^{eff}}\right) \times n} \quad \forall\ i,\ k \quad (4)$$

Where, ϕ_{avg}^{k} is the average surface normal angle of k^{th} strip, $\left|\phi_{S_i^k}\right|_{eff}$ is the effective average surface normal angle measured on i^{th} contour section fall in k^{th} strip calculated by the Equation 4, $P_{S_i}^{k}$ is the area generated by i^{th} projected contour section fall in k^{th} strip, N_i^k is the number of points on the i^{th} contour section fall in k^{th} strip which is determined rationally based on the percentage area of i^{th} contour in k^{th} strip and n is a integer and can be defined as resolution for ϕ_{avg}^{k}. Finally by determining the surface normal angle for each strip, the distance between filaments in individual strip can be determined by using Equation 5 to counteract the change in material concentration due to the deformation.

$$L_1^k = \frac{\pi R_1}{2(1 - Porosity_{Desired})} Cos\phi_{avg}^{k} \quad (5)$$

Where, L_1^k is the space between fibres in k^{th} strip, R_1 is the deposited filament radius which depends upon fabrication system capability, $Porosity_{Desired}$ is the desired porosity level in the membrane. By determining the filament distance for all the strips, the filament deposition location for the first layer is completed. The same methodology has been applied for consecutive layer using strips parallel to the filament lay-down pattern and layer independent design parameters.

2.3 ANALYZE AND EVALUATION OF THE DESIGNED MEMBRANE

Due to the free-form wound surface, a quadrilateral pore-cell concept [8] is more appropriate for measuring the porosity by combining both layer in such deformed condition shown in Figure 4. Because of the free form wound shapes the generated quadrilateral pore-cells are highly anisotropic in nature. And due to this variation, the porosity in each pore-cell needs to be measured by using the following equation.

$$Porosity_{i,i+1,j,j+1}^{porecell} = 1 - \frac{\pi(R_2^{i\,2} A_4 + R_2^{j\,2} A_3 + R_2^{i+1\,2} A_2 + R_2^{j+1\,2} A_1)}{Area\_A_1A_2A_3A_4 \times 8 \times R_1} \quad \forall\ i,j \quad (6)$$

Where, $Porosity_{i,i+1,j,j+1}^{porecell}$ is the porosity of the pore-cell generated by i^{th} and $(i+1)^{th}$ filament of first layer and j^{th} and $(j+1)^{th}$ filament of consecutive layer. Similarly, R_2^i, R_2^{i+1}, R_2^j and R_2^{j+1} are the deformed radius for i^{th}, $(i+1)^{th}$, j^{th} and $(j+1)^{th}$ filament respectively. Also, A_1 is the segment length of $(j+1)^{th}$ filament falls between i^{th} and $(i+1)^{th}$ filament of first layer as shown in the following Figure 4(a). Similarly, A_2, A_3 and A_4 are the segment of $(i+1)^{th}$, j^{th} and i^{th} filament respectively.

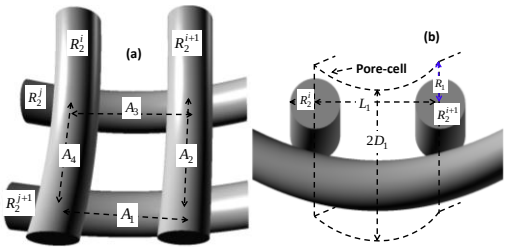

Figure 4: *Pore-cell and deformed porosity calculation.*

To quantify the effectiveness of the proposed method, a percentage area based porosity evaluation index (PPEI) has been used [1] by using the following equation.

$$PPEI = \sum_{-i}^{i} \frac{CellArea\_Porosity_{DP(1+ni)\sim DP(1+n(i+1))}}{Wound\_Area} \times \frac{|ni| + |n(i+1)|}{2} \quad \forall\ i:\ i \in \mathbf{Z},\ n > 0 \quad (7)$$

Where, DP is the desired porosity, n is the percentage increment factor, $CellArea\_Porosity_{DP(1+ni)\sim DP(1+n(i+1))}$ is the total surface area of the deformed pore-cell that has resultant porosity within the $DP(1+ni) \sim DP(1+n(i+1))$ range and $Wound\_Area$ is the wound surface area, $\frac{|ni| + |n(i+1)|}{2}$ is the penalty factor which is proportional to the resultant porosity deviation.

3 IMPLEMENTATION

The methodology has been implemented to a multi-basin, non-convex free-form surface profile as virtual wound shape shown in Figure 5 which has been generated by using NURBS based Rhino 4.0. The contour line shows the free-form surface profile along its depth which is taken 0.4 mm apart. The generated surface has two basins as shown in Figure 5 and the maximum depth lies around first basin (Basin 1) with 4.6 mm. The depth for the other basin (Basin 2) is 3.5mm. The maximum width and length is 15.5 mm and 35 mm respectively. A two layers 0^0-90^0 layout pattern membrane with constant desired porosity and cylindrical shape filament assumption has been generated by both conventional and proposed design method using the same Rhinoceros 4.0 and Visual-Basic Script. The membranes are placed over the virtual wound surface and uniform axial load has been applied on them to resemble the dressing load which might cause shape conforming deformation of the membrane. This

deformation modelling has been performed in Abaqus 6.9 by matching the hydrogel bio-material properties. Then the deformed membrane are used for porosity analysis applying the methodology described in section 2 and colour legend surface have been used to visualize the resultant porosity comparison in both conventional and proposed membrane design.

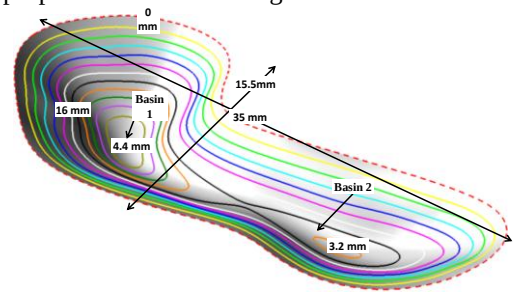

Figure 5: *A multi-basin free form virtual wound shape and its contour along the depth.*

Table 1. *Design parameter and PPEI comparison for the multi-basin free-form surface presented in Figure 5.*

% Designed Porosity, P	Filament Diameter, D mm	$L=\frac{\pi D}{4(1-P)}$, mm	Proposed method: Vertical Strip Number	Proposed method: Horizontal Strip Number	Proposed method: Slice Distance, h mm	d_SL+h	PPEI	Conventional Method PPEI
55	100	0.235	35	16	0.3	5.5 L	2.9	9.4

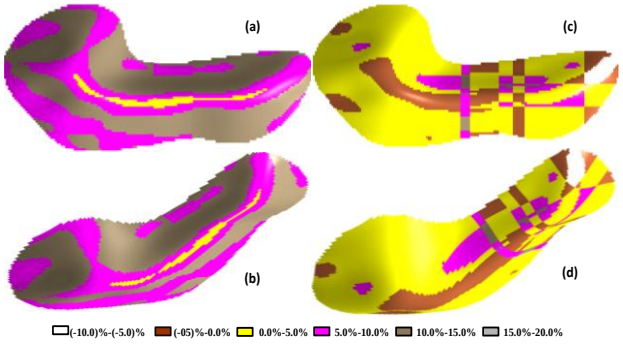

Figure 6: *Porosity comparison on two layer membrane with 60% porosity and 60 µm filament radius (a-b) top view and perspective view for conventional fixed filament distance (c-d) top view and perspective view for proposed variational filament distance respectively (color legend represent the % deviation from the designed porosity).*

In the conventional equidistant filament method, 60% porosity requires 65 horizontal filaments and 147 vertical filaments with radius of 60 µm. On the other hand the proposed method for variational distance requires 75 and 167 filament respectively. In case of conventional membrane 55.1% of its area shows 10%-15% higher porosity and 36% of its area shows 5%-10% higher porosity than the designed porosity (60%), which might be significant. But by using the proposed method for the same surface, a total 85.2% of its surface area has a resultant porosity within ±5% of the target and the resultant porosity for rest of the area shows 5%-10% higher than designed porosity as shown in Figure 6. More over the PPEI value with the proposed model is significantly lower than the value obtained from conventional equidistant filament membrane as show in Table 1.

4 CONCLUSION

The proposed design has transformed the equidistant filament membrane into variational distance filament membrane to minimize its deformation effect. Even though the difference in deformed and desired porosity may not be eliminated completely in a free form complex surface, but this proposed novel modelling technique would give more control on desired porosity level over the scaffold structure for performing its preferred functionality with higher accuracy.

REFERENCES

[1] A. Khoda and B. Koc, "Deformable Porosity for Multi-Functional Tissue Scaffolds," *ASME Transactions, Journal of Medical Device (Submitted)*, 2011.

[2] B. Balakrishnan, *et al.*, "Evaluation of an in situ forming hydrogel wound dressing based on oxidized alginate and gelatin," *Biomaterials*, vol. 26, pp. 6335-6342, 2005.

[3] S. Levenberg and R. Langer, "Advances in Tissue Engineering," in *Current Topics in Developmental Biology*. vol. Volume 61, P. S. Gerald, Ed., ed: Academic Press, 2004, pp. 113-134.

[4] H. Hong, *et al.*, "Fabrication of Biomatrix/Polymer Hybrid Scaffold for Heart Valve Tissue Engineering in Vitro," *ASAIO Journal*, vol. 54, pp. 627-632 10.1097/MAT.0b013e31818965d3, 2008.

[5] K. W. Ng, *et al.*, "Assimilating cell sheets and hybrid scaffolds for dermal tissue engineering," *Journal of biomedical materials research. Part A*, vol. 75A, pp. 425-437, 2005.

[6] W. H. Eaglstein, "Moist Wound Healing with Occlusive Dressings: A Clinical Focus," *Dermatologic Surgery*, vol. 27, pp. 175-182, 2001.

[7] SAXENA, *et al.*, *Vacuum-assisted closure: Microdeformations of wounds and cell proliferation. Discussion* vol. 114. Hagerstown, MD, ETATS-UNIS: Lippincott Williams & Wilkins, 2004.

[8] A. Khoda, *et al.*, "A functionally gradient variational porosity architecture for hollowed scaffolds fabrication," *Biofabrication*, vol. 3, pp. 1-15, 2011.

[9] J. M. Sobral, *et al.*, "Three-dimensional plotted scaffolds with controlled pore size gradients: Effect of scaffold geometry on mechanical performance and cell seeding efficiency," *Acta Biomaterialia*, vol. 7, pp. 1009-1018, 2011.

[10] A. K. M. B. Khoda, *et al.*, "Engineered Tissue Scaffolds With Variational Porous Architecture," *Journal of Biomechanical Engineering*, vol. 133, p. 011001, 2011.